UNCLASSIFIED

AD NUMBER
ADB967408
LIMITATION CHANGES
TO: **Approved for public release; distribution is unlimited. Document partially illegible.**
FROM: **Distribution authorized to DoD only; Administrative/Operational Use; 27 DEC 1948. Other requests shall be referred to Air Materiel Command, Wright-Patterson AFB, OH 45433. Pre-dates formal DoD distribution statements. Treat as DoD only. Document partially illegible.**
AUTHORITY
WRDC ltr dtd 20 Dec 1990

THIS PAGE IS UNCLASSIFIED

THIS REPORT HAS BEEN DELIMITED
AND CLEARED FOR PUBLIC RELEASE
UNDER DOD DIRECTIVE 5200.20 AND
NO RESTRICTIONS ARE IMPOSED UPON
ITS USE AND DISCLOSURE.

DISTRIBUTION STATEMENT A

APPROVED FOR PUBLIC RELEASE;
DISTRIBUTION UNLIMITED.

UNANNOUNCED
DTIC FILE COPY

UNCLASSIFIED

AD-B967 408

Technical Report
distributed by

DEFENSE TECHNICAL INFORMATION CENTER

DTIC
ELECTE
MAR 30 1990
S B D

DTIC Acquiring Information – Imparting Knowledge

Defense Logistics Agency
Defense Technical Information Center
Cameron Station
Alexandria, Virginia 22304-6145

UNCLASSIFIED

90 03 30 003

UNCLASSIFIED

NOTICE

We are pleased to supply this document in response to your request.

The acquisition of technical reports, notes, memorandums, etc., is an active, ongoing program at the **Defense Technical Information Center (DTIC)** that depends, in part, on the efforts and interest of users and contributors.

Therefore, if you know of the existence of any significant reports, etc., that are not in the **DTIC** collection, we would appreciate receiving copies or information related to their sources and availability.

The appropriate regulations are Department of Defense Directive 3200.12, DoD Scientific and Technical Information Program; Department of Defense Directive 5230.24, Distribution Statements on Technical Documents *(amended by Secretary of Defense Memorandum, 18 Mar 1984, subject: Control of Unclassified Technology with Military Application)*; American National Standard Institute *(ANSI)* Standard Z39.18, Scientific and Technical Reports: Organization, Preparation, and Production; Department of Defense 5200.1R, Information Security Program Regulation.

Our Acquisition Section, **DTIC-FDAB**, will assist in resolving any questions you may have. Telephone numbers of that office are:

(202) 274-6847, (202) 274-6874 or Autovon **284-6847, 284-6874.**

DO NOT RETURN THIS DOCUMENT TO DTIC

EACH ACTIVITY IS RESPONSIBLE FOR DESTRUCTION OF THIS DOCUMENT ACCORDING TO APPLICABLE REGULATIONS.

UNCLASSIFIED

Reproduced by

UMENT SERVICE CENTER
VICES TECHNICAL INFORMATION AGENCY
BUILDING, DAYTON, 2, OHIO

4580

en Government or other drawings, specifications or
used for any purpose other than in connection with
lated Government procurement operation, the U.S.
ereby incurs no responsibility, nor any obligation
d the fact that the Government may have formulated,
any way supplied the said drawings, specifications
not to be regarded by implication or otherwise as
licensing the holder or any other person or corpora-
any rights or permission to manufacture, use or
inventi n that may in any way be related thereto."

CLASSIFIED

AF Technical Report 5747

A.T.I. No. 44580

STUDIES ON HEAT TRANSFER IN LAMINAR FREE CONVECTION WITH THE ZEHNDER-MACH INTERFEROMETER

UNITED STATES AIR FORCE
AIR MATERIEL COMMAND
Wright-Patterson Air Force Base
Dayton, Ohio

Date: 27 December 1948

UNITED STATES AIR FORCE
AIR MATERIEL COMMAND
WRIGHT-PATTERSON AIR FORCE BASE
DAYTON, OHIO

TECHNICAL REPORT
No. 5747

STUDIES ON HEAT TRANSFER IN LAMINAR FREE CONVECTION WITH THE ZEHNDER-MACH INTERFEROMETER

By

E. R. G. Eckert
and E.E. Soehngen

Edited by F. J. Keating

Approved:

R. J. Minty, Colonel, USAF
Chief, Power Plant Laboratory

For the Commanding General:

for Carl F. Damberg Col USAF
Fred R. Dent, Jr.
Colonel, USAF
Chief, Engineering Operations
Engineering Division

Laboratory No.	MCREXP
E. O. No.	535-51
No. of Pages	21
No. of Figures	34

Accession For	
NTIS GRA&I	☐
DTIC TAB	☐
Unannounced	☑
Justification	
By	
Distribution/	
Availability Codes	
Dist	Avail and/or Special
12	

QUALITY INSPECTED 4

TABLE OF CONTENTS

	Page No.
Introduction	1
Evaluation of Interference Photos	1
End Effects	6
The Vertical Plate	7
Two Parallel Vertical Plates	9
Horizontal Cylinder	13
Horizontal Cylinder with Square Cross-Section	15
Arrangements of Horizontal Cylinders	16
Two Concentric Cylinders	18
Convection Caused by Centrifugal Forces	19
Summary	20
Bibliography	21

LIST OF ILLUSTRATIONS

Fig. No.	Title	Page
1	Schematic sketch of the interferometer.	1
2	Interference photo of free convection on a horizontal cylinder.	2
3	Temperature profile near the surface of a solid body.	4
4	Temperature field around a horizontal plate.	4
5	Logarithmic plot of a temperature profile.	4
6	Boundary layer on a flat plate.	5
7	Determination of the boundary layer thickness	5
8	End effects in two-dimensional problems (isotherms around a corner).	6
9	Temperature variation along light rays near the end of a horizontal cylinder.	7
10	Interference photo of a horizontal cylinder with its axis normal to the light rays.	7
11	Isotherms around a vertical plate.	8
12	Temperature profiles on a vertical plate.	8
13	Temperature profile on a vertical plate in reduced scale.	9
14-16	Isotherms around two heated vertical plates.	10
17	Isotherms around a heated and an unheated vertical plate.	11
18	Temperature profiles on two heated vertical plates.	12
19	Non-dimensional heat transfer coefficient on two heated vertical plates.	12
20	Temperature profiles on a heated and an unheated vertical plate.	13
21	Velocity profiles on two heated vertical plates.	13
22	Isotherms around a horizontal heated cylinder in free convection.	13
23	Local non-dimensional heat transfer coefficient along the circumference of a horizontal cylinder (dashed line according to E. Hermann).	14
24	Temperature profile on a horizontal cylinder in reduced scale.	14
25-26	Isotherms around a horizontal cylinder with square cross-section.	15
27	Local non-dimensional heat transfer coefficient on a horizontal cylinder with square cross-section with a diagonal vertical.	15
28	Local non-dimensional heat transfer coefficient on a horizontal cylinder with square cross-section with two sides vertical.	16
29	Isotherms around two horizontal cylinders.	16
30	Isotherms around three staggered horizontal cylinders.	17
31	Local non-dimensional heat transfer coefficient around the circumference of two horizontal cylinders. (I lower cylinder, II upper cylinder).	17
32	Local non-dimensional heat transfer coefficient around the circumference of three staggered horizontal cylinders. (I lowest, II medium, III upper cylinder).	18
33	Isotherms in the space between two concentric horizontal cylinders.	18
34	Local non-dimensional heat transfer coefficient around the circumference of two concentric horizontal cylinders. (I inner, II outside cylinder).	19

STUDIES ON HEAT TRANSFER IN LAMINAR FREE CONVECTION WITH THE ZEHNDER-MACH INTERFEROMETER

1. Introduction

A Zehnder-Mach interferometer was built in the Power Plant Laboratory of the Air Materiel Command in Wright-Patterson Air Force Base for the purpose of investigating heat transfer, fluid flow, and mixing phenomena occurring in aircraft power plants. The instrument has glass plates 8 inches in diameter and a useful span of 32 inches.[1] The present paper gives the results of studies with this instrument on heat transfer in laminar free convection. These studies were started since they could be accomplished with very simple equipment which could be procured with a minimum delay. They presented, therefore, a very convenient means to check the accuracy of the instrument and to become familiar with its use. Apart from this, however, there are also immediate applications of free convection heat transfer in modern aircraft power plants, for instance all cooling or insulating problems connected with the handling of fuels for jets and rockets. In the course of the studies it was also found that valuable information can be obtained on turbulence, its nature and beginning. The results of studies dealing with heat transfer in turbulent free convection will be presented in a separate report. Data on thermal convection flow are useful also in understanding radial flow phenomena which are caused by centrifugal forces in turbo compressors and turbines. This analogy will be investigated in more detail in Chapter 9 of this report.

Some earlier work was done with the interferometer in the field of heat transfer. R. B. Kennard[2] published in 1931 the results of studies on free convection heat transfer on a vertical plate and a horizontal cylinder. He used for his experiments a Zehnder-Mach interferometer with a field of view 1 by 3/4 inches in size. A later paper[3] describes essentially the same experiments with a few additional tests on two parallel vertical plates. A short note on the use of the Zehnder-Mach interferometer for the study of temperature fields in air was published by L. A. Randas and E. K. Paranjpe[4] in 1936. A similar reference is contained in papers by G. Hansen[5] and H. Schardin[6]. Some experiments, up to now unpublished, on a vertical plate and a horizontal cylinder in natural convection were conducted by E. Groth at Wright-Patterson Air Force Base, who used an interferometer built by Th. Zobel.

2. Evaluation of Interference Photos

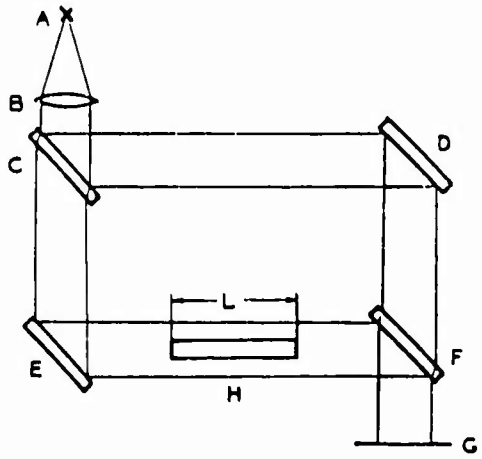

Fig. 1 - Schematic sketch of the interferometer

Fig. 1 shows a schematic sketch of a Zehnder-Mach interferometer. Monochromatic light from a mercury lamp A is made parallel by a lens B. On the glass plate C which is coated in such a way that it transmits half of the light and reflects the other half it is divided into two bundles. One is reflected on the mirror D the other one on mirror E and both are united again by a second glass plate F coated in the same way as plate C. On a screen G behind the plate F this light shows interference phenomena. When the plates and mirrors C to F are exactly parallel then the field on the screen is uniformly dark or bright depending on whether the path lengths of the two light bundles differ by an even or odd number of half wave lengths thus causing the light waves of the two bundles to be in phase and amplify or to be out of phase and extinguish each other. If, however, two of the plates are turned through a slight angle, then a succession of dark and light fringes appears on the screen G since the difference of the two path lengths varies from place to place. In the work described in this report the first adjustment was used where the plates are all parallel to each other. When in this adjustment the object H to be investigated -- for instance a heated horizontal cylinder with its length L in the direction of the light rays -- is brought into one light bundle of the instrument as indicated in Fig. 1 then a picture can be observed on the screen as shown in Fig. 2.

Fig. 2 - Interference photo of free convection on a horizontal cylinder

Around the shadow of the cylinder, dark interference fringes appear in the field which was uniformly bright before. These fringes are caused by the fact that the optical refraction coefficient of the air has changed in the heated zone surrounding the hot cylinder. The amount of this change of the refraction coefficient on any place can be determined from the interference photo. The refraction coefficient is by definition the ratio of the velocity of light in vacuum to the velocity in the medium investigated or, what is equivalent, the ratio of the two corresponding wave lengths.

As an equation it can be written

$$n = \frac{\lambda_0}{\lambda} \qquad (1)$$

where n is the refraction coefficient λ_0 the wave length in vacuum, and λ the wave length in the investigated medium. Now on any ray the number ν of light waves in the length L of the investigated object is

$$\nu = \frac{L}{\lambda} \qquad (2)$$

The number ν_r of waves in the same length on a reference light ray outside the heated zone is

$$\nu_r = \frac{L}{\lambda_r} \qquad (3)$$

Therefore the difference ε in the number of waves on both rays is

$$\varepsilon = \nu_r - \nu = L\left(\frac{1}{\lambda_r} - \frac{1}{\lambda}\right) \qquad (4)$$

or using the refraction coefficients instead of the wave lengths

$$\varepsilon = \frac{L}{\lambda_0}(n_r - n) \qquad (5)$$

This difference ε in the number of waves can on the other hand be determined from the interference photo (Fig. 2). It is easily seen that it equals the number of interference fringes between the reference point where the refraction coefficient is n_r, and the point in question where the refraction coefficient is n, when the four plates C to F are adjusted parallel to each other. With the number of interference fringes counted from an arbitrary reference point in the interference photos we can therefore determine by equation (5) the difference in the optical refraction coefficient between any point in the photo and the reference point.

Now there exists a relation between the optical refraction coefficient of a medium and its specific weight γ. This connection is according to L. Lorenz and H. A. Lorentz

$$\frac{n^2-1}{n^2+2}\,\frac{1}{\gamma} = const \qquad (6)$$

The value of the constant depends essentially only on the nature of the molecules by which the medium is built up but not on the phase (liquid or gaseous). For mixtures it is built up additatively by the values of the single weight components as long as there are no chemical reactions between them. For gases the value of the refraction coefficient is nearly 1. We can then simplify equation(6)in very good approximation to

$$\frac{n-1}{\gamma} = C \qquad (7)$$

wherein C is a constant for any gas within reasonable limits of pressure and temperature. The optical refraction coefficient n_0 of dry air at 32°F and 29.2 inches mercury column for green light with the wave length $\lambda_0 = 0.5461\mu$ ($1\mu = 1/1000$ mm) which was used in our experiments is 1.0002934.[7] This gives for the constant in equation 7 the numerical value 0.003625 ft^3/lb or in the metric system 0.0002263 m^3/kg. In humid air the refraction coefficient varies slightly. It can be determined from an equation given by Lorenz

$$n_h = n_{dr} - 5.5 \times 10^{-8}\,\pi \qquad (8)$$

where n_h is the refraction coefficient for humid air, n_{dr} for dry air at the same temperature and π the vapour pressure in mm mercury column.

With equations 5 and 7 it is possible to calculate the difference between the specific weight γ at any point in the interference photo and the specific weight γ_r at a reference point. We get from 7

$$\gamma = \frac{1}{C}(n-1)$$

and $$\gamma_r - \gamma = \frac{1}{C}(n_r - n) \qquad (9)$$

With equation 5 this gives

$$\gamma_r - \gamma = \frac{\lambda_0}{CL}\,\varepsilon \qquad (10)$$

In the photo, Fig. 2, it is convenient to use the zone outside the heated layer around the tube as reference point. Equation (10) shows that the change in specific weight at any point within the heated layer is proportional to the number of interference fringes as counted from the outside to this point as long as the length L of the light ray in the zone of changed density is constant. For two - dimensional problems investigated in this report this is the case.* On any of the fringes the specific weight is therefore constant. In free convection problems the velocities and therefore the pressure differences are so small that their influence on the specific weight can be neglected. The specific weight changes only with temperature and the interference fringes in Fig. 2 are therefore isotherms. With the adjustment of the interferometer where all plates are parallel the interference photo shows immediately the isotherms in two-dimensional convection problems. The whole field of isotherms is contained in one photo which can be taken with a very short exposure time. This is a great advantage of the interference method.

In forced convection flow with higher velocities the pressure as well as the temperature varies generally within the air stream. In this case the evaluation of an interference photo gives only the field of the specific weight and the measurement of a second variable (pressure or temperature) is necessary in order to determine the state of the fluid in any point. Within the boundary layers, however, the pressure is with sufficient accuracy constant on normals to the surface on which the boundary layer is built. On these normals, therefore, the specific weight of the fluid or gas depends only on temperature and the interference photo gives the temperature field in this zone. This fact makes the interferometer especially apt for heat transfer investigations.

The temperature on any of the interference fringes in a field where the pressure can be regarded as constant may be calculated from equation (10) and the gas law

$$T = \frac{p}{R}\frac{1}{\gamma} \qquad (11)$$

introducing γ from (10) into this equation gives

$$T = \frac{p}{R}\frac{1}{\gamma_r\left(1 - \frac{\lambda_0 \varepsilon}{CL\gamma_r}\right)} = T_r \frac{1}{1 - \frac{\lambda_0 \varepsilon}{CL\gamma_r}} \qquad (12)$$

with T_r the absolute temperature and γ_r the specific weight on the reference point (outside the heated layer). The second summand in the denominator is usually small as compared with 1 . Therefore, it is more convenient to convert the fraction into a series

$$T = T_r\left[1 + \frac{\lambda_0 \varepsilon}{CL\gamma_r} + \left(\frac{\lambda_0 \varepsilon}{CL\gamma_r}\right)^2 + \left(\frac{\lambda_0 \varepsilon}{CL\gamma_r}\right)^3 \cdots\right] \qquad (13)$$

The temperature difference $\Delta T = T - T_r$ thus becomes

$$\Delta T = T_r\left[\frac{\lambda_0 \varepsilon}{CL\gamma_r} + \left(\frac{\lambda_0 \varepsilon}{CL\gamma_r}\right)^2 + \left(\frac{\lambda_0 \varepsilon}{CL\gamma_r}\right)^3 + \cdots\right] \qquad (14)$$

With this equation the temperature fields in the present report were calculated. Actually it was only necessary to use the first two or three summands of the series. The constants used were: $\lambda_0 = 0.5461 \times 10^{-3}\,mm$, $C = 0.003625\,\frac{ft^3}{lb}$. The length L of the investigated objects was approximately 12 inch. All studies were done in air with a temperature T_r near $80°F = 540°K$ and at normal barometric pressure. The number ε of fringes was counted in the interference photo.

The most important value for heat transfer calculations is the heat transfer coefficient. The local film heat transfer coefficient h on the surface of a solid body can be determined from the interference photo in the following way. According to the definition of this coefficient it is connected with the heat flow q through the surface perunit area and a characteristic temperature difference ΔT which has to be agreed to for every problem by the equation

$$q = h\Delta T \qquad (15)$$

On the other hand it follows from the fact that the air in the immediate neighborhood of the solid surface is at rest relative to this surface and the heat is transported by conduction through this air layer that

$$q = k_w\left(\frac{dT}{dy}\right)_w \qquad (16)$$

where k_w is the heat conductivity of the air at the wall temperature and y is the direction normal to the surface or $(dT/dy)_w$ the temperature gradient within the air on the surface. It is advantageous to build a dimensionless expression with the film heat transfer coefficient, the Nusselt number

*It is sometimes difficult for actual tests to fulfill this condition. The next section deals with this problem in detail.

$$Nu = \frac{hD}{k} \qquad (17)$$

D is a characteristic dimension (for the circular cylinder the diameter). It is a question still open today at which temperature the conductivity k of the air should be introduced into this expression. Previous investigators used mostly the conductivity at wall temperature for free convection problems. If we follow this usage then equations (15) to (17) result in

$$Nu = \frac{D}{\Delta T}\left(\frac{dT}{dy}\right)_w \qquad (18)$$

The temperature gradient $(dT/dy)_w$ on the surface can be determined from the temperature profile, Fig. 3.

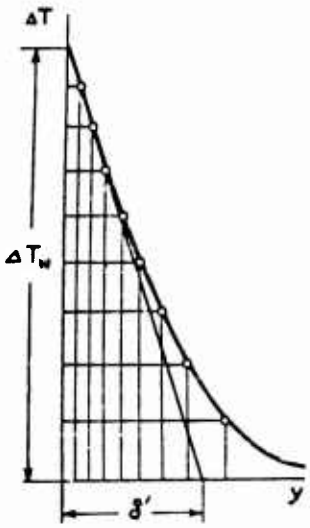

Fig. 3 - Temperature profile near the surface of a solid body.

This profile is obtained from the interference photos by measuring the distance of the interference fringes from the surface on that point where the local heat transfer coefficient is to be determined and plotting the temperatures calculated with equation (14) over these distances. The subtangent to this profile denoted by δ' in Fig. 3 is

$$\delta' = \frac{\Delta T}{(dT/dy)_w} \qquad (19)$$

Introducing this into equation (18) gives

$$\boxed{Nu = \frac{D}{\delta'}} \qquad (20)$$

It can be seen that the Nusselt number is simply the ratio of two lengths of which one is predetermined as reference length used for the special problem whereas the second can be obtained from the temperature profile. This makes the determination of the heat transfer coefficients by the interferometer very convenient.

The accuracy of this method of determining the Nusselt number depends on the accuracy with which the tangent can be drawn on the temperature profile. On a surface whose radius of curvature is not too small the temperature profile is nearly a straight line immediately on the surface because the layer adjacent to the surface behaves like a straight solid wall and the heat is therefore transported by conduction.

Fig. 4 - Temperature field around a horizontal plate.

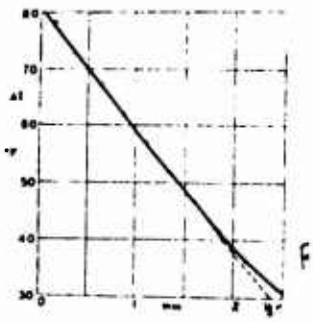

Fig. 5 - Logarithmic plot of a temperature profile.

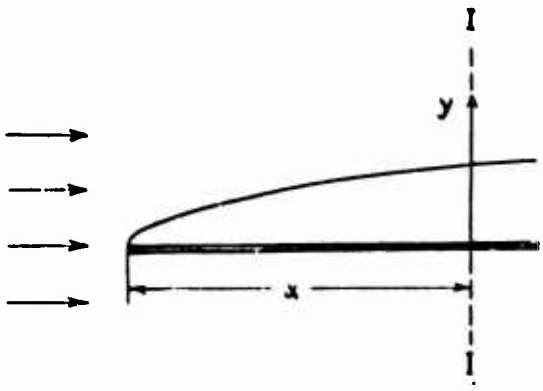

Fig. 6 - Boundary layer on a flat plate.

The tangent can be drawn with accuracy on such profiles. On a surface with a small radius of curvature the innermost airlayer behaves like a cylindrical solid layer, and it is better to plot the temperatures over the logarithm of the distance from the surface. Then the part of the temperature profile near the surface becomes a straight line and permits an exact determination of the tangent. Fig. 4 shows the temperature field around a horizontal plate and Fig. 5 presents the temperature profile on a horizontal line at the right hand end of this plate. It can be seen that the first seven points of the temperature curve lie on a straight line and determine the tangent with accuracy.

In forced convection flow at high Reynolds numbers the boundary layers are very thin when the high Reynolds numbers are obtained by great velocities on comparatively small objects. Then determining the tangent becomes inaccurate especially in turbulent boundary layers where the temperature profile is straight only within the very thin laminar sublayer. In some cases the heat transfer coefficient must then be determined in another way. Fig. 6 is a sketch which indicates how the boundary layer develops on a flat plate. When the plate is warmer than the medium flowing along it then it gives off heat to this medium. All the heat which the plate lost on its length x must be contained in the flow which passes the plane I - I. With the average film heat transfer coefficient $\bar{h}$ for the length x, the heat flow Q per unit time from the same plate length

$$Q = \bar{h} x \Delta T_w = \int_0^\infty \gamma c_p V \Delta T dy \qquad (21)$$

where ΔT is the temperature difference at the distance y from the plate within the boundary layer as compared with the outside undisturbed flow, V is the velocity within the boundary layer at the place where the temperature difference is ΔT, γ is the specific weight, c_p is the specific heat at constant pressure of the flowing medium, and ΔT_w is the difference in temperature between the wall and the undisturbed flow. In most cases the specific weight γ and the specific heat c_p can be assumed constant throughout the boundary layer. Solving for $\bar{h}$ and multiplying both sides of the equation by the velocity V_0 in the undisturbed flow gives

$$\frac{\bar{h}}{\gamma c_p V_0} = \frac{1}{x V_0 \Delta T_w} \int_0^\infty V \Delta T dy \qquad (22)$$

The dimensionless grouping on the left hand side of the equation is an expression well known in the heat transfer field. It is the St-function as used by Colburn, or with the dimensionless values of the Nusselt number $Nu = \frac{\bar{h} x}{k}$, Reynolds number $Re = \frac{V_0 x}{\nu}$, and Prandtl number $Pr = \frac{\nu}{a}$, it is

$$\overline{St} = \frac{\overline{Nu}}{Re\, Pr} = \frac{1}{x V_0 \Delta T_w} \int_0^\infty V \Delta T dy \qquad (23)$$

In order to solve this equation the velocity profile and the temperature profile must be known. The latter can be obtained from an interference photo in the way described before for free convection flow. The velocity profile is to be obtained in another way. The knowledge of the velocity profile is not necessary where the flowing medium has a Prandtl number equal to one, and the tubbulent exchange coefficient is equal for heat and momentum. In this case the velocity profile is similar to the temperature profile and can be derived by the equation

$$\frac{V}{V_0} = 1 - \frac{\Delta T}{\Delta T_w} \qquad (24)$$

Introducting this into equation (23) leads to

$$\overline{St} = \frac{1}{x} \int_0^\infty \frac{\Delta T}{\Delta T_w} \left(1 - \frac{\Delta T}{\Delta T_w}\right) dy \qquad (25)$$

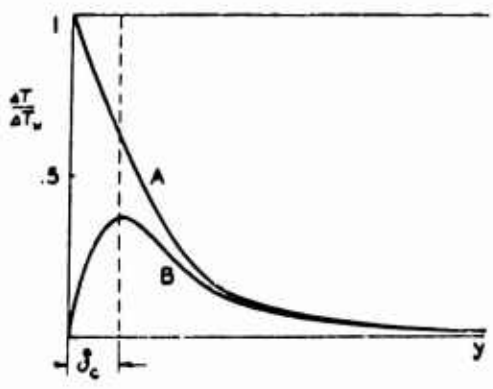

Fig. 7 - Determination of the boundary layer thickness

In Fig. 7 the temperature profile as it is obtained from an interference photo is shown as curve A. Multiplying each value $\Delta T/\Delta T_w$ with the corresponding $1-\Delta T/\Delta T_w$ gives curve B. The area under this curve is the integral in equation (25).

This integral has the dimension of a length. We may, therefore regard it as a kind of boundary layer thickness and call it δ_c. A corresponding procedure with the velocity profile leads to a boundary layer thickness which is known as "impulse thickness". It can be seen that the dimensionless grouping $Nu/Re\,Pr$ can again be expressed as the ratio of two lengths: the thermal boundary layer thickness δ_c and the distance measured along the plate.

$$\overline{St} = \frac{\overline{Nu}}{Re\,Pr} = \frac{\delta_c}{x} \qquad (26)$$

The thermal boundary layer thickness is defined generally by the integral $\int_0^\infty \Delta T/\Delta T_w\, dy$. For the case where the Prandtl number is one, the turbulent exchange coefficient for heat and momentum are equal, and no essential accelerations occur in the flow, [illegible] be transformed into $\int \Delta T/\Delta T_w (1-\Delta T/\Delta T_w)\, dy$.

Gases have a Prandtl number which does not differ much from the value 1. For these media therefore the described method should give satisfactory results on surfaces where no strong accelerations or decelerations of the flow occur. First it is necessary to check its accuracy, however.

3. End Effects.

In deriving equations (10) and (11) it was assumed that the light ray which travels along the investigated object (Fig. 1) passes through an air layer of uniform temperature and specific weight on the whole length L, and that on the rest of its way the specific weight of the air is the same as on a corresponding ray which has a greater distance from the investigated object and does not enter the heated zone around it. This means that the temperature in the air suddenly drops in the two planes coinciding with the end surfaces of the investigated object to its outside value. This is the condition which should be fulfilled at the investigation of two-dimensional problems but it is difficult to realize it in actual experiments. Two methods were used to keep these end effects small.

In previous investigations the heated object was put into the light path in the way as indicated in Fig. 1. The end surfaces which are normal to the light rays also give off heat to the surrounding air and the heated zone --the thermal boundary layer of the air closes around those end surfaces. Along a light ray near the surface the air temperature does not drop suddenly at the end surface as it should but decreased gradually within the boundary layer. This gives an error in the evaluation of the interference photo whose magnitude has to be evaluated. It was mentioned previously that the air in the zone immediately at the surface of the investigated object is at rest and the temperature field in this zone is the same as connected with heat condution in a solid body. Such a temperature field which can be determined by conformal mapping should therefore be a reasonable approximation for the real temperature field within the whole boundary layer. Fig. 8 shows the isotherms around a rectangular corner determined by conformal mapping taken from reference 8.

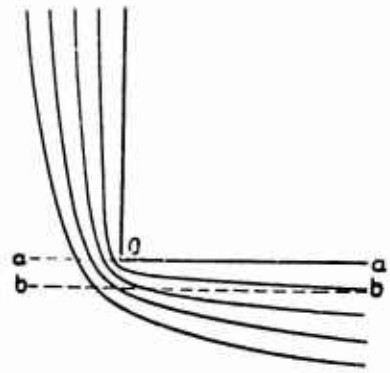

Fig. 8 - End effects in two-dimensional problems (isotherms around a corner)

We will study the end effect on a horizontal cylinder in free convection with the help of this figure which may represent a corner between the cylindrical surface and one of the end planes of the cylinder. A light ray a-a tangential to the cylinder surface or a light ray b-b near to the surface (Fig. 8) passes through regions with decreasing temperature near the corner. A certain temperature can be assigned to any of the isotherms in Fig. 8 by the assumption that in moving above the cylinder to a great distance from the corner they should asymptotically coincide with the temperature profile known for the cylinder by measurement and calculation (Fig. 17). Now from Fig. 8 the temperatures can be determined on any light ray. Thus the temperature curves in Fig. 9 were obtained for light rays at different distances from the cylinder wall. The temperatures are plotted over the distance in mm from the end plane (5.74 in). The curves show how the temperature decreases gradually near the ends of the cylinder instead of the sudden jump in the end plane. The number ε of the fringes in the interference photos which is determined by equation (5) when the specific weight drops suddenly is given by

$$\varepsilon = \frac{C}{\lambda_0}\int(\gamma_r - \gamma)\,dL \qquad (2\text{[illegible]})$$

when the specific weight changes gradually. For the purpose of estimating the error by end effects only the first term in equation (14) can be used with sufficient accuracy to transform this into

$$\varepsilon = C\gamma_r \int (\gamma_r - \gamma)\,dL \qquad (27)$$

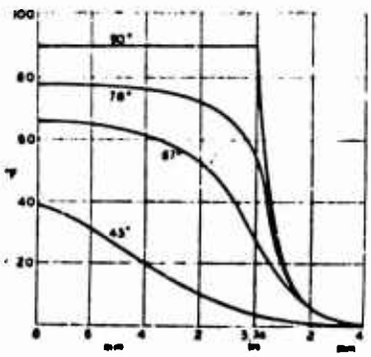

Fig. 9 - Temperature variation along light rays near the end of a horizontal cylinder.

The integral can be obtained for any light ray with the help of Fig. 9 and in this way the error introduced by the assumption of a sudden change in temperature in the end plane and by the use of equation (10) or (14) can be determined. For the length L = 11.46 inch used in the tests of the horizontal cylinder the error in determining the temperatures from the interference photo is +0.5% for the light ray touching the cylinder surface, 0% for the light ray 1/2 mm distant from the surface, -0.5% for the light ray in 1mm distance and -2.5% for the ray in 2mm distance. Determining the heat transfer coefficient from the slope of the temperature profile introduces in this example an error of +3%.

A qualitative picture of the end effects can be obtained from an interference photo where the investigated object is placed with its axis normal to the light ray direction. Such a photo for the horizontal cylinder is shown in Fig. 10.

Fig. 10 - Interference photo of a horizontal cylinder with its axis normal to the light rays.

Another method to reduce end effects is to put two glass windows against the two end surfaces. This works satisfactorily as long as the glass windows are not heated excessively by the investigated object. Heated glass plates disturb the interference pattern by the inner tension in the glass and by the deformation of its surfaces which accompanies the unequal heating. The heating of the plates can be reduced by an insulation between the heated investigated object and the plate, or by making the thickness of the glass plates as small as possible. A thin glass plate reduces the inner tensions in the glass and the effect of the deformation of the surfaces on the interference pattern. The Optron Laboratory, Dayton, Ohio, succeeded in manufacturing glass plates of 8 inches diameter and 1/8 inch thickness of such quality that only a very slight change in the interference pattern could be observed when the plates were put into the light path of the interferometer. A local heating of these plates changed the interference pattern only to a degree which was deemed admissable for the purpose of this investigation. To decrease the heating a cork layer of approximately 1/6 inch thickness was put between the end surfaces of the investigated object and the glass plates. This method of reducing the end effects was used for some of the experiments.

4. The Vertical Plate.

The temperature field and heat transfer on a heated vertical plate in natural convection was investigated very thoroughly experimentally and by calculation by E. Schmidt, W. Beckmann and E. Pohlhausen[10]. This problem therefore is well suited to checking the accuracy

of the interferometric method for heat transfer experiments. Interference photos were made of a copper plate 5 inches high, 5/32 inches thick and with a length L = 24 in. in the light ray direction. The plate was heated on a hot plate. Its heat capacity was high enough to keep it warm for about one quarter of an hour. Since the whole temperature field around the plate is contained in one interference photo which is taken with approximately one hundredth of a second exposure time the slowly decreasing temperature of the plate does not affect the accuracy of the measurements. This, incidentally, is an advantage of the interference method. In the above mentioned investigation the temperature field was measured with thermocouples and the measurement took several days. To keep the temperature of the plate and the surrounding constant during this time was rather difficult. Fig. 11 is an interference photo, showing the isotherms around the plate.

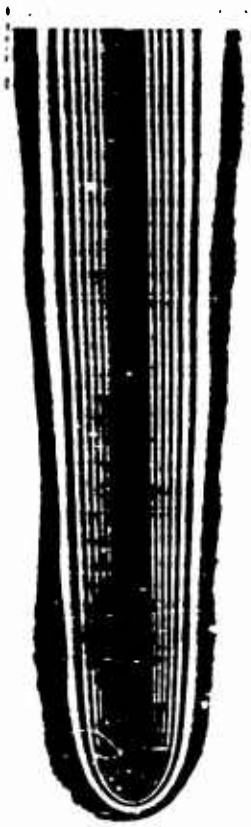

Fig. 11 - Isotherms around a vertical plate.

The heated zone and the thermal boundary layer along the plate can be observed very clearly. On an infinitely thin plate the boundary layer begins according to theory with the thickness zero on the lower edge and increases proportional to the fourth root of the distance from this edge. The finite thickness of the plate is the reason for the fact that in Fig. 11 the boundary layer begins with a certain thickness on the lower plate edge. The temperature profiles on normals to the plate surface at different distances from the lower edge were determined from the interference photo by the method described in Section 2. Figure 12 shows these profiles for a temperature difference ΔT_w of 90°F. between the plate and the air at a great distance (outside the boundary layer).

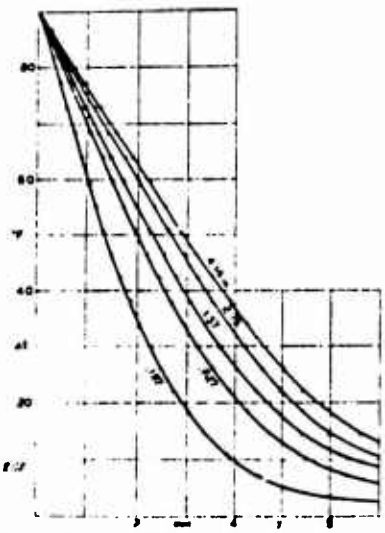

Fig. 12 - Temperature profiles on a vertical plate.

The temperatures are plotted over the distance y from the plate and the parameter on the curves is the distance of the normal from the lower plate end. Such temperature profiles were determined also for temperature differences ΔT_w of 17, 24, 35, 58.5 and 85.8°F.

E. Pohlhausen[10] deduced from the boundary layer equations for free convection flow that the temperature profiles in a dimensionless form, as the ratio of the temperature difference ΔT at any point of the profile to the temperature difference ΔT_w on the wall, depend only on one dimensionless variable $C\frac{y}{\sqrt{x}}$, where y is the distance from the plate on a normal to the surface, x the distance of the normal from the lower plate edge and $C = \sqrt[4]{\frac{g\,\Delta T_w}{\nu^2 T_r}}$ with g the acceleration of gravity, $\Delta T_w = T_w - T_r$ the wall temperature, T_r the temperature of the surrounding air undisturbed by the plate and ν the kinematic viscosity of the air. By plotting the temperature ratio $\Delta T/\Delta T_w$ over the value $Cy/\sqrt{x}$ all the temperature profiles

should come together into one single curve. Fig. 13 shows such a plot.

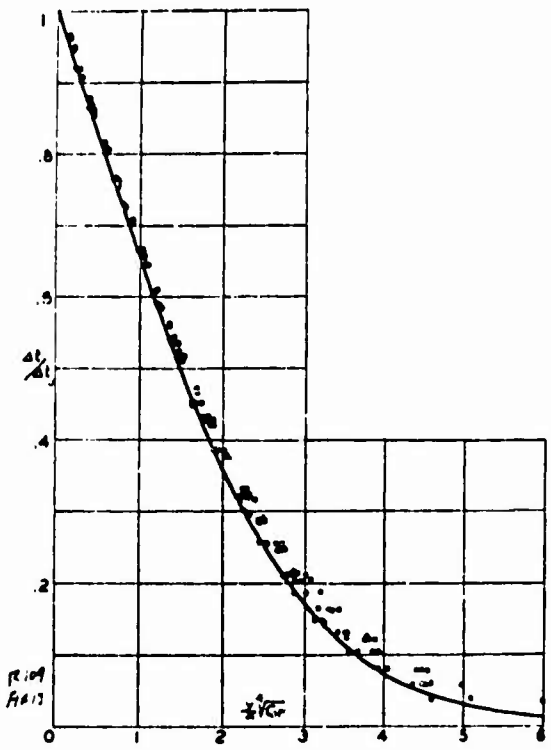

Fig. 13 - Temperature profile on a vertical plate in reduced scale.

The constant C was determined with the kinematic viscosity ν at an average temperature of 113°F. To be exact the reference temperature for the viscosity changes with the temperature difference, even when the room temperature is constant. But since we do not know yet which reference temperature is to be used (wall temperature or some mean between wall and room temperature) and since the influence of the variation of the viscosity on the value C is very small at the small temperature differences realized in the experiments a constant value 113°F of the reference temperature was used. It can be observed that the measured points lie close together on one curve. The scattering is slightly greater in the outside part, and is probably due to a slight turbulence in the room which is very difficult to avoid. The solid line shows the temperature profile calculated by E. Pohlhausen[10] and the agreement between it and the measurements is excellent. For the average film heat transfer coefficient $\bar{h}$ on a vertical plate with the height x (in inches) in air, E. Schmidt and W. Beckmann[10] derived from their experiments the formula

$$\bar{h} = K\sqrt[4]{\frac{\Delta T_w}{T_r x}}\sqrt{\frac{b}{29.9}} \qquad (28)$$

where ΔT_w is the difference between the plate temperature and the temperature of the outside air and b the barometric pressure of the air in inches mercury. They found from their experiments the value for the constant K was 1.24. The calculation of E. Pohlhausen[10] gave 1.21 and our experiments 1.165 with a deviation of ±3% in the single measurements. For a general use of heat transfer data it is more desirable to present the data in a dimensionless form. The Nusselt number $Nu = hD/k$ with a length D characteristic for the special problem is given as a function of other dimensionless variables. Dimensional analysis reveals that for free convection these independent variables are the Grashof number $Gr = g\beta_r \Delta T_w D^3/\nu^2$ with the expansion coefficient β and the Prandtl number $Pr = \nu/\alpha$ with the thermal diffusivity α. For gases the expansion coefficient is equal to the reciprocal value of the absolute temperature $\beta_r = 1/T_r$. If the function is restricted to air the Prandtl number has a constant value and the Grashof number is the only independent variable. The calculated equation for air in this representation is

$$\overline{Nu} = C\sqrt[4]{Gr}, \quad \overline{Nu} = \frac{\bar{h}x}{k}, \quad Gr = \frac{g\,\Delta T_w x^3}{T_r \nu^2} \qquad (29)$$

with $C = 0.420$ from theory, 0.492 from E. Schmidts and 0.463 from our experiments. It is known from other investigations that this equation is valid for $10^4 < Gr < 10^9$. Summing up it can be stated that the consistancy of these interferometric investigations on the vertical plate among themselves and the agreement with the theory is as good or even better than the very careful experiments by E. Schmidt and W. Beckmann.

5. Two Parallel Vertical Plates.

Knowing the heat transfer from a single vertical plate it is of interest to learn when and how much it is influenced by walls in the neighborhood. To study this problem the temperature field in air at free convection on two parallel vertical plates was determined. Either both of the plates were heated up to the same temperature or only one plate was heated the other being approximately at the same temperature as the surrounding air. Only a few experimental results are found in the literature and they do not solve the problem generally. In our experiments two copper plates were used which had the same dimension as the single plate in the experiments mention-

ed in the preceeding section. They were heated in the same way. The distance between both plates was varied (0.209, 0.233, 0.426 and 0.600 in) for the two heated plates. Only one distance (0.246 in) was investigated for the heated and cold plate. Figs. 14 to 16 show the temperature field around two heated plates and Fig. 17 presents the isotherms around a heated and a cold plate.

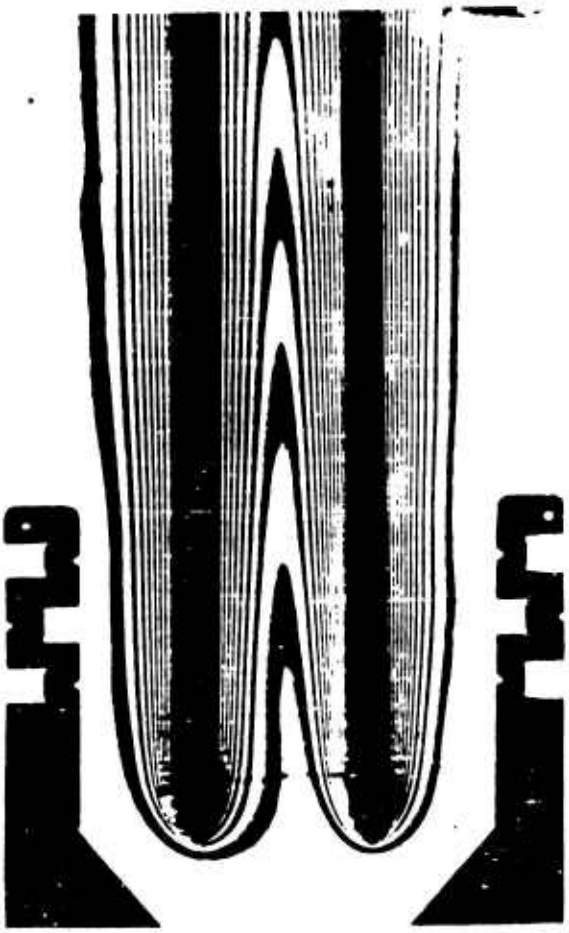

Fig. 14 - Isotherms around two heated vertical plates.

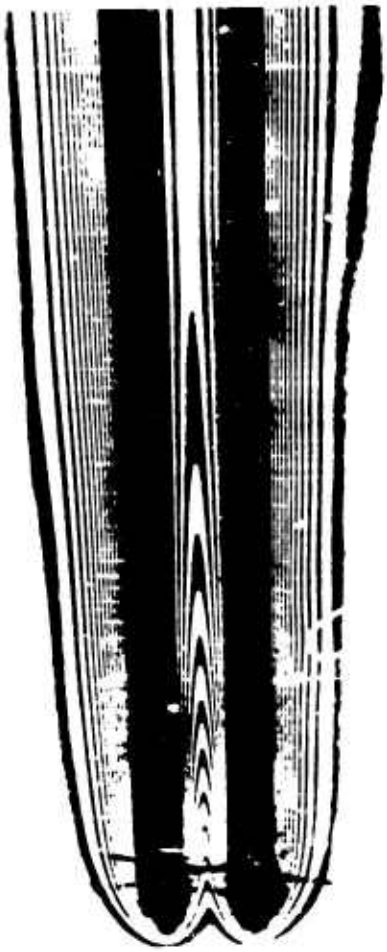

Fig. 15 - Isotherms around two heated vertical plates.

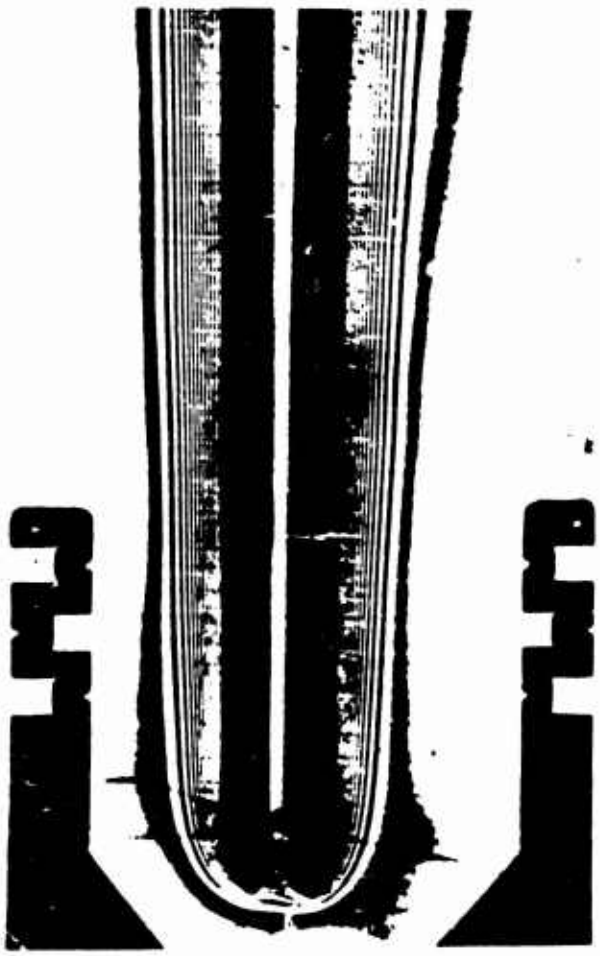

Fig. 16 - Isotherms around two heated vertical plates.

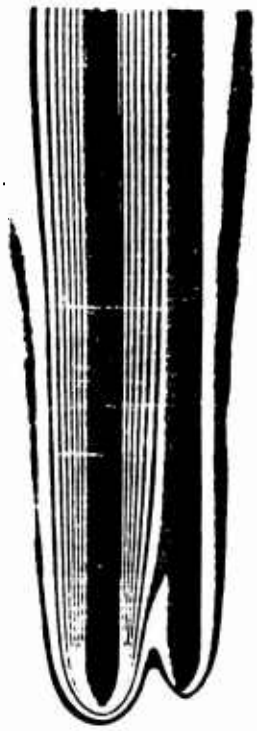

Fig. 17 - Isotherms around a heated and an unheated vertical plate.

It can be seen from the photos that the boundary layers start with the same shape on the exterior and the interior sides of the plates in the vicinity of the lower plate edges. On the outside of the plates the boundary layers have the same shape as on a single plate for the whole plate height. On the sides of the plates, however, which face each other they are influenced more and more by the presence of the second plate as the distance from the lower plate edge increased. The process is similar to the inflow into a tube or channel between two parallel planes. The influence of the second plate on the boundary layer can be observed most clearly in a diagram in which the temperature profiles at difference distances x from the lower plate edge are plotted over

the reduced dimensionless distance from the plate $Ky/\sqrt[4]{x}$ or what is equivalent $y/x\sqrt[4]{Gr}$.

On the single vertical plate this plotting brings all the temperature profiles together into one single line as shown in Fig. 13. Fig. 18 shows the temperature profiles with this plotting for two heated plates with two different distances d from each other.

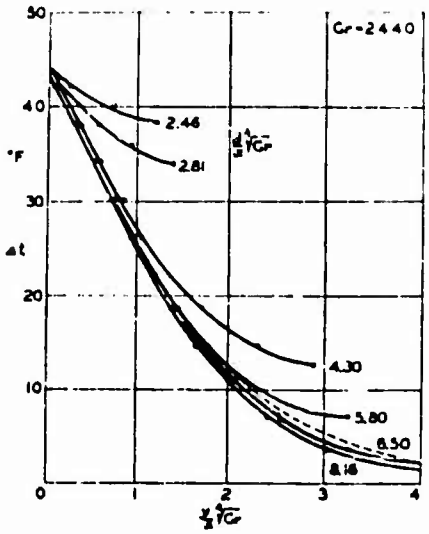

Fig. 18 - Temperature profiles on two heated vertical plates.

The curves end in points which correspond to half the distance between the two plates. The dashed curve is the one into which all the temperature curves fall together on the outside of the plates. The Grashof numbers in the figure are built with the value x as characteristic length. It can be seen that the presence of the second plate changes the shape of the temperature profile only near the outside of the boundary layer as long as the distance of the plates in the reduced scale $d/x\sqrt[4]{Gr}$ is great. The heat flow from the plate is influenced by the second plate only when the temperature gradient changes. In Fig. 18 this is the case for the two upper-most profiles. The readings at the other plate distances are not included in the diagram because they would make the plot too crowded. They were, however, used for the evaluation of the heat transfer coefficients (Fig. 19). The local film heat transfer coefficient can be determined from the gradient of the temperature profiles on the plate surface in Fig. 18. In Fig. 19 the value $Nu/\sqrt[4]{Gr}$ is plotted over the distances of two plates in the reduced scale.

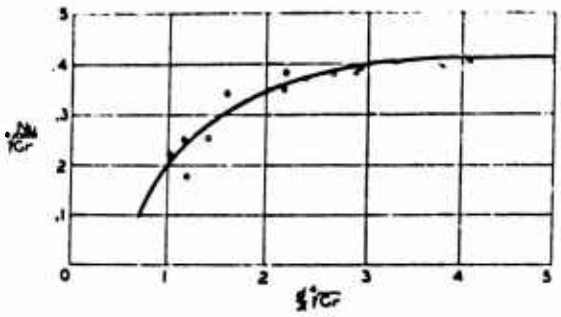

Fig. 19 - Nondimensional heat transfer coefficient on two heated vertical plates.

According to equation (29) the value $Nu/\sqrt[4]{Gr}$ is constant for a single vertical plate in air. It is therefore represented by a horizontal straight line in Fig. 19. The readings for two parallel plates show how the heat flow from the plates is influenced when the distance between the two plates decreases. The curve drawn through the points seems to approach the asymptotic value .405 which is 10% higher than the value $Nu/\sqrt[4]{Gr}$ built with the local heat transfer coefficient for the single plate. It may be that a slight convection in the room was the reason for this difference. Generally the accuracy of the measurements on the single plate is higher than for the two plates since many more photos were evaluated for the first case. A limiting distance x_ℓ where the influence of the second plate begins to be felt can be determined in Fig. 19. Of course, there exists no sharply defined value for it since the nondimensional heat transfer coefficient decreases gradually when the distance between the plates becomes smaller. We may regard the value $d/x\sqrt[4]{Gr} = 3.5$ where the heat transfer coefficient begins to decrease as the limiting value. This gives

$$\frac{x_\ell}{d} = \frac{1}{3.5}\sqrt[4]{Gr} \qquad (30)$$

with

$$Gr = \frac{g\,\Delta T_w\,x^3}{\nu^2\,T_r} \qquad (31)$$

With this equation the ratio of the limiting length x_ℓ to the distance of the two plates may be calculated. It can be assumed that equation (31) is valid between the same limits as equation (29) namely, for $10^4 < Gr < 10^9$. Fig. 20 shows the temperature profiles on two parallel vertical plates of which only one plate is heated. At the distance of the two plates investigated no influence of the cold plate is felt by the heated plate in regard to the heat flow. When the distance of the two plates is smaller than the heat transfer on the

hot plate is increased by the presence of the second plate whereas it is decreased on two heated plates. More plate distances would have to be investigated to determine the limiting length for this plate pair, but, it seems that the value is approximately the same as on the two heated plates. As a first approximation the equation (30) can be used also for this case.

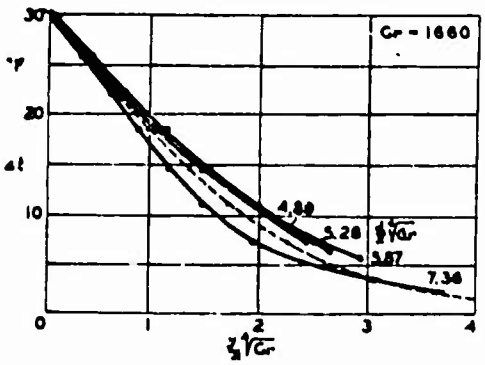

Fig. 20 - Temperature profiles on a heated and an unheated vertical plate.

The velocity profile on a single vertical plate was measured by E. Schmidt and W. Beckmann[10]. The shape of this profile is shown in Fig. 21 as solid line A.

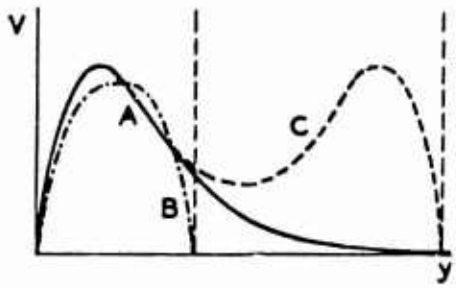

Fig. 21 - Velocity profiles on two heated vertical plates.

On two parallel heated plates the velocity profile is changed as shown in line C as long as the limiting length is not exceeded. At the limiting length the distance of the plates is 3.5 times the distance of the velocity maximum from the plate surface. At small reduced distances the shape of the velocity profile changes gradually to curve B.

The two vertical plates were investigated without glass plates closing the span between the two plates on both sides. At first it was supposed that by a "chimney effect" lower pressures could build up between the plates and suck in air from both sides in this way disturbing the two-dimensional flow. However, interference photos of two plates with their planes normal to the light ray direction revealed that this was not the case within the range of plate heights and distances investigated.

6. Horizontal Cylinder.

Temperature profiles on a heated horizontal cylinder at free convection in air were measured with thermoelements by different investigators[11]. A calculation of the temperature and velocity field around the horizontal cylinder was presented by R. Hermann[12]. Interferometric studies on this shape are therefore useful to check the accuracy of this method. A solid copper cylinder with 0.578 in diameter and 11.46 inches length was heated before the tests. Its heat capacity was high enough to keep it hot for the time needed for the photographs. Figs. 2 and 22 show such photos revealing the isotherms around the cylinder. From these photos the temperature gradients on normals to the cylinder surface and the local film heat transfer coefficients were determined in the way described in Section 2.

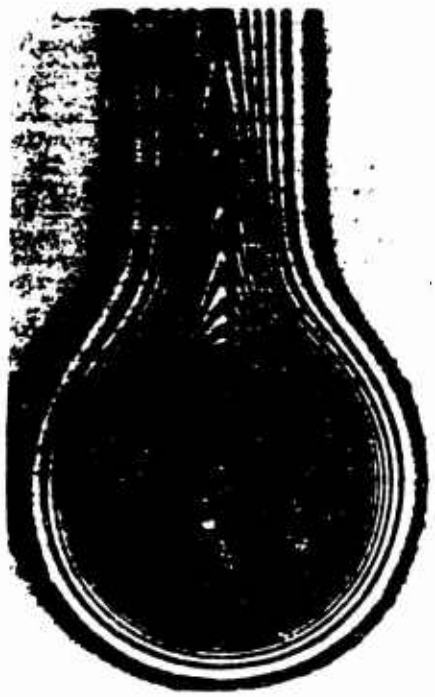

Fig. 22 - Isotherms around a horizontal heated cylinder in free convection.

Fig. 23 shows these local heat transfer coefficients plotted over the angle as measured

from a vertical drawn through the cylinder center in downward direction.

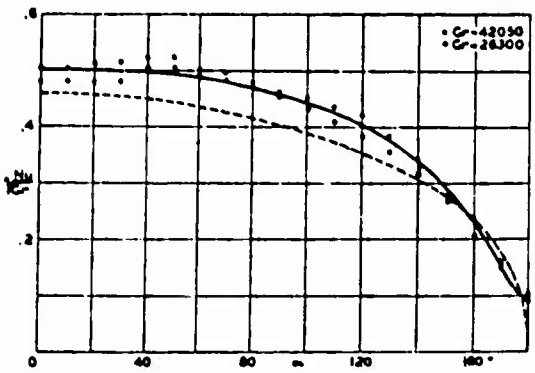

Fig. 23 - Local nondimensional heat transfer coefficient along the circumference of a horizontal cylinder (dashed line according to R. Hermann).

Two interference photos taken with a temperature difference of the cylinder to the surrounding air of 44.5 and 93.37 were evaluated. The Grashof numbers for both test sets are recorded in the diagram. Since the calculation of R. Hermann showed that the value $Nu / \sqrt[4]{Gr}$ depends for air within a wide range of Gr numbers only on the position on the cylinder circumference this value is used as ordinate in Fig. 23. The property values of air were inserted into the dimensionless Nu and Gr numbers at the cylinder surface temperature. The diagram also shows the dimensionless local film heat transfer coefficient calculated theoretically by R. Hermann as a dashed line. It may be observed that both the measured and the calculated values agree quite well, the measured points lying in the average 10% above the calculated ones. The same is true for the average film heat transfer on the cylinder surface. From our experiments the equation

$$\overline{Nu} = 0.401 \sqrt[4]{Gr} \qquad (32)$$

is derived, whereas the theory gives 0.372 for the numerical value. Both dimensionless values are built with the cylinder diameter as characteristic length. Since other measurements (summarized by R. Hermann[12]) gave also values for the average film heat transfer coefficient which were 10% above the theoretical one and since this difference cannot be explained by the uncertainty at which temperature the property values should be introduced the reason for the deviation is probably the fact that the thickness of the boundary layer is assumed as small compared with the cylinder diameter in the theory. Figs. 2 and 22 show that the boundary layers are quite thick at the investigated Gr- numbers. Higher Gr- numbers which are connected with thinner boundary layers should give a still better agreement with theory. According to previous measurements the formula 32 is valid for $10^4 < Gr < 10^9$

At Grashof numbers greater than 10^9 the boundary layer becomes turbulent. For smaller values than 10^4 the thickness of the boundary layer is so great that the boundary layer theory cannot be applied any longer. The theory shows also that all the temperature profiles measured at different angles should fall together into a single one when the scale for the abscissa values is reduced using a distribution-function $f(\alpha)$ given by R. Hermann which is equal to the ratio of the theoretical local heat transfer coefficient at the angle investigated to the theoretical heat transfer coefficient at the angle $\alpha = 0$. Fig. 24 shows the ratio of the temperature difference within the boundary layer to the difference of the wall temperature to the outside air temperature plotted over this reduced scale.

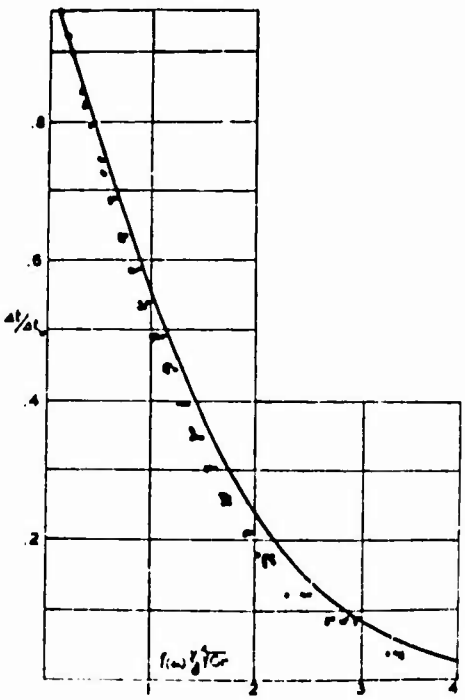

Fig. 24 - Temperature profile on a horizontal cylinder in reduced scale.

It can be observed that all the measured points lie very closely on a single curve. The solid curve in the figure is the calculated temperature profile. All the measurements lie somewhat beneath this curve. The same thing was true for the temperature profiles measured by K. Jodlbauer[11]. Summarizing it can be stated that the agreement between the theory of G. Hermann and our measurement is good and the agreement between our measurements and the ones by K. Jodlbauer is excellent.

7. Horizontal Cylinder with Square Cross-Section

A horizontal heated cylinder with square cross-section at free convection in air was investigated in two positions: with one diagonal of the square vertical or with two side planes vertical. The dimensions of the cylinder were: 0.969 in. length of each side of the square and 11.5 in. cylinder length. The cylinder was heated in the same way as in the previous experiments. Figs. 25 and 26 show the field of isotherms around the cylinder, and Figs. 27 and 28 present the local film heat transfer coefficients plotted over the circumference of the cylinder.

Fig. 25 - Isotherms around a horizontal cylinder with square cross-section.

Fig. 26 - Isotherms around a horizontal cylinder with square cross-section.

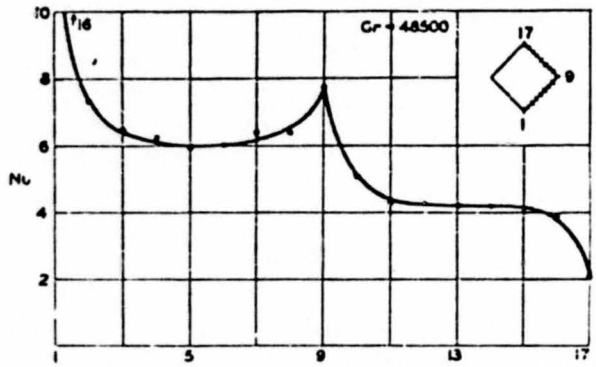

Fig. 27 - Local nondimensional heat transfer coefficient on a horizontal cylinder with square cross-section with a diagonal vertical.

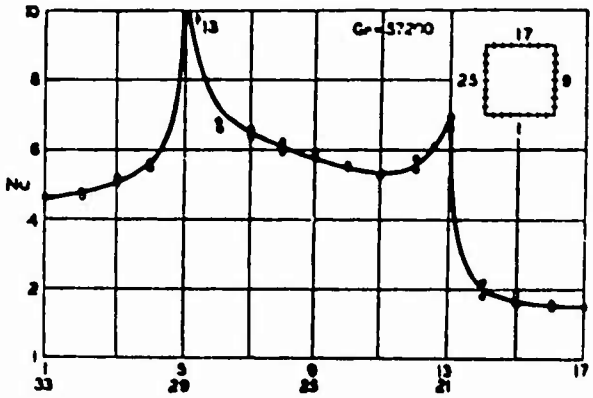

Fig. 28 - Local nondimensional heat transfer coefficient on a horizontal cylinder with square cross-section with two sides vertical.

The Grashof numbers are added in both diagrams. Interesting are the high local values of the heat transfer coefficient at the edges. The average film heat transfer coefficients were determined by planimetering. The value for this is $\overline{Nu} = 5.61$ for the position with vertical diagonal and $\overline{Nu} = 5.08$ for the position with vertical side. Assuming that the Nusselt number varies with the fourth root of the Grashof number for these cylinders also, a fact which may be deduced from the analogy to the horizontal circular cylinder and the vertical plate, the following equations can be derived for the average Nusselt numbers at free convection in air. Horizontal cylinder with square cross-section one diagonal of which is vertical:

$$\overline{Nu} = 3.27\sqrt[4]{Gr} \qquad (33)$$

Horizontal cylinder with square cross-section two sides of which are vertical:

$$\overline{Nu} = 4.54\sqrt[4]{Gr} \qquad (34)$$

The Nu and the Gr number are built with the side length of the square. The limits of the Grashof number within which the equations are valid are not yet known but probably similar to the ones for the cylinder with circular cross-section and the vertical plate. The upper limit may be somewhat lower than for the horizontal circular cylinder. For the position with vertical diagonal the average heat transfer coefficient is greater, for the position with vertical sides smaller, than on a horizontal cylinder with circular cross-section of the same diameter provided the temperatures are always the same.

8. Arrangements of Horizontal Cylinders.

Heat exchangers utilizing free convection heat transfer are often composed of horizontal tubes. If some of the tubes are arranged above others they are mutually influenced in their heat transfer since the warm air stream rising from the lower tubes hits the upper ones. No thorough investigation of this problem is known to the authors. To investigate it the interference photos shown in Figs. 29 and 30 were taken.

Fig. 29 - Isotherms around two horizontal cylinders.

The dimensions of the cylinders were the same as the one used in the tests described in Section 6.

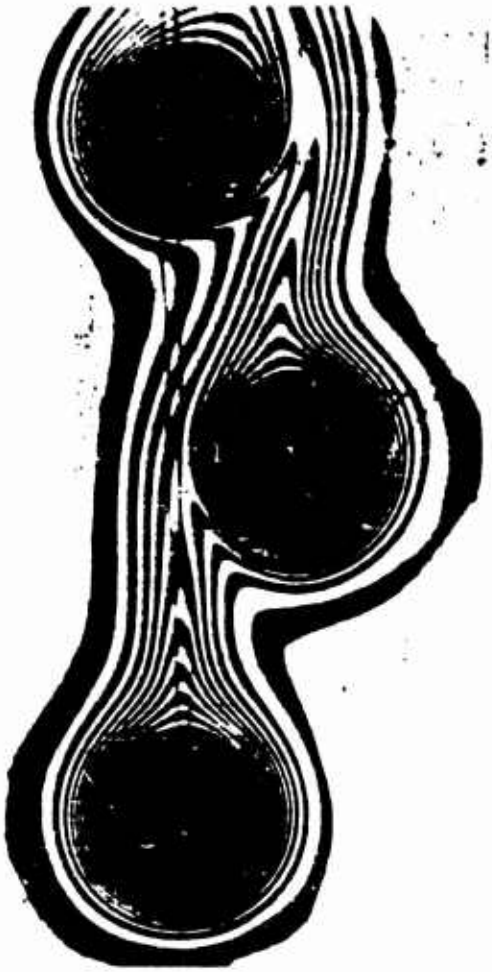

Fig. 30 - Isotherms around three staggered horizontal cylinders.

The distribution of the nondimensional local film heat transfer coefficient, the Nusselt number, over the circumference is represented in Fig. 31 for two horizontal cylinders one above the other. The Nusselt number is built with the cylinder diameter. The heat transfer on the lower cylinder is the same as for a single horizontal one. For the upper cylinder however the heat transfer coefficient has a peak at the place where the warm air stream hits its surface.

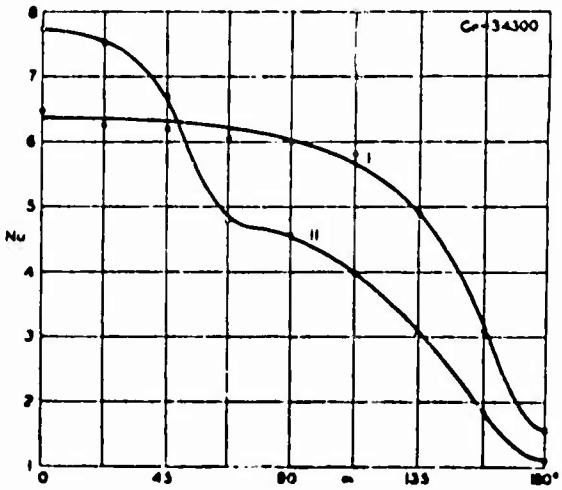

Fig. 31 - Local nondimensional heat transfer coefficient around the circumference of two horizontal cylinders. (I lower cylinder, II upper cylinder).

There are two influences acting in opposite directions: the higher air velocities within this warm air wake tend to increase the heat flow from the surface of the second cylinder, but the higher air temperatures there decrease the temperature difference and tend to decrease the heat transfer. The influence of the higher velocity is the stronger one in the region of impingement, the lower temperature difference is the determining factor on the sides of the cylinder. The average heat transfer coefficient on the cylinder surface is found by planimetering. It is $Nu = 5.30$ for the lower and $Nu = 4.62$ for the upper cylinder. The average heat transfer coefficient on the upper cylinder decreased therefore to 87% of the heat transfer on the lower one.

The same investigation on three horizontal cylinders above each other resulted in the statement, that the heat transfer on the second cylinder was 83% and on the third one 65% of the heat transfer on a single cylinder.

Since the average heat transfer is decreased when the wake of another cylinder hits the surface it can be concluded that the effectiveness of a heat exchanger can be increased by staggering the tubes. Fig. 30 shows the isotherms around the cylinders in such an arrangement and Fig. 32 presents the Nusselt number in its distribution around the circumference of the three cylinders.

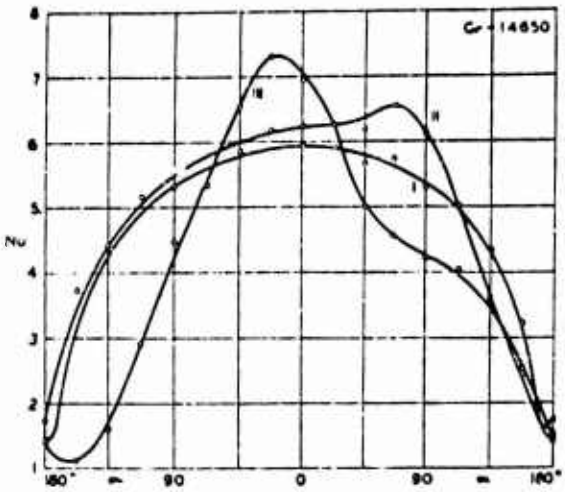

Fig. 32 - Local nondimensional heat transfer coefficient around the circumference of three staggered horizontal cylinders. (I lowest, II medium, III upper cylinder).

Again the peak in the heat transfer coefficients can be observed on both the middle and the upper cylinder. The average heat transfer coefficient of the middle cylinder is 10[illegible]% and the one on the upper cylinder 87% of the heat transfer on the lowest one. The heat transfer on the lowest cylinder has again the same value as on a single horizontal cylinder. By the staggered arrangement the heat flow on the middle and the upper cylinders was increased appreciably as compared with the arrangement of the cylinders above each other.

9. Two Concentric Cylinders

It is well known that gases are the best media for thermal isolation as long as convection currents are prevented within them since gases have the lowest value of the heat conductivity. An isolation method utilizes this fact by arranging aluminum foils in certain distances around the body to be isolated. The air layers between these foils keep the heat losses down. The simplest shape of such an isolation with air layers is the space between two concentric cylinders. As far as is known the temperature field and the local heat transfer on such an enclosed air space was measured never before. For this reason interference photos were made, an example of which is shown in Fig. 33.

Fig. 33 - Isotherms in the space between two concentric horizontal cylinders.

A solid copper cylinder with 0.882 inches diameter is arranged concentrically within a thick walled copper tube with 1.89 in. inner diameter. The cylinders are 11.62 inches long and their axis are horizontal. The inner cylinder is held centrally by three thin pins on each end. The shadows of the pins are visible in the photo.. Both ends of the tube were closed by glass windows 1/8 inch thick. The inner cylinder was brought into the tube after being heated and it kept warm long enough for the experiments. Two cork discs 1/6 in. thick on the cylinder ends diminished the heat flow to the windows.

Fig. 33 reveals the interesting fact that in the enclosed air space boundary layers build up along the surfaces. A hot boundary layer moves around the inner cylinder, rises from its highest point, hits the outer tube and in moving along its surface cools down again. The heat transfer is high on places where the interference lines crowd together in the vicinity of a surface indicating a steep temperature gradiant. On the lower side of the inner cylinder and on the upper side of the outer tube are places of great heat flow. On the lower side of the outer tube the heat transfer is very low. In the space between the two boundary layers there is a temperature increase in upward direction. It may be mentioned that the interferometer was adjusted for a uniform field without lines by making the four basic glass plates parallel to each other.

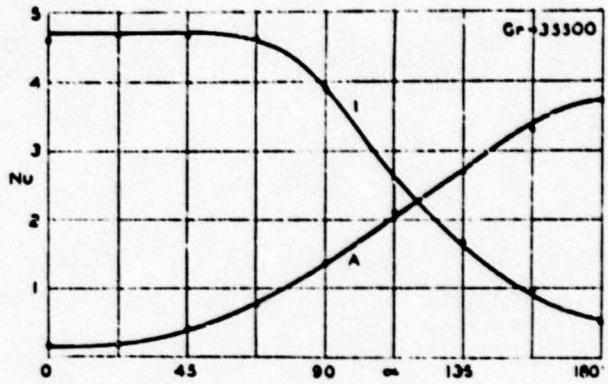

Fig. 34 - Local nondimensional heat transfer coefficient around the circumference of two concentric horizontal cylinders. (I inner, A outside cylinder).

Fig. 34 shows the local film heat transfer coefficients around the inner and the outer surface of the ring shaped space. It can be seen that the heat flow is distributed very unevely around both cylinders. The dimensionless film heat transfer coefficient Nu was computed with the temperature difference between both cylinder surfaces and each one with the corresponding cylinder diameter. The Grashof number given in the diagram was built with the diameter of the small cylinder. The average Nusselt number found by planimetering is 1.60 for the outer and 3.22 for the inner cylinder diameter. A test can be made for the accuracy of the measurement. Neglecting heat losses through the glass and plates the heat flow from the inner cylinder must equal the heat flow to the outer tube or the product conductivity of the air at wall temperature times Nusselt number times diameter sould give the same value on the inner and outer wall. From the interference photo we get for the product the value 16.9 on the outer and 17.2 on the inner wall which differ by 2%.

10. Convection caused by Centrifugal Forces

In all the problems studied in the proceeding chapters the actuating force for the movement in free convection was gravity. In turbo engines (compressors and turbines) and other rotating machinery physical processes occur on some places which are very similar to the ones studied above with the exception that centrifugal forces replace the gravitational force. An example is the gas turbine with liquid cooled blades according to E. Schmidt[14]. The blades have radial cylindrical holes which are filled with water. The layers in the water adjacent to the walls are heated and the density is decreased in this way. Therefore, the centrifugal forces are smaller on these particles than in the central core which remains cooler and in this way intensive convection currents are generated which produce a very good cooling effect. Also on turbines with aircooled hollow blades such currents occur and may participate appreciably in the cooling effect. The physical process is exactly the same as the one generated in a geometrically similar model with free convection caused by gravity as long as the Grashof and the Prandtl numbers have the same value in both cases. In this way the cooling effect can be studied on a simple stationary model. In the process which involves centrifugal forces the Grashof number must be built with the centrifugal acceleration U^2/r (U circumferential velocity, r distance from the axis of revolution) instead of the gravitational acceleration g. It is therefore

$$Gr = \frac{(U^2/r)\beta \Delta T \ell^3}{\nu^2} \qquad (35)$$

There are other flow phenomena in turbo engines which are, if not of exactly the same nature, at least very similar to thermal free convection processes. For their understanding the study of free convection flow is therefore very helpful[15]. In axial compressors and turbines boundary layers develop on the blades. On the stator blades the circumferential velocity and the centrifugal forces are much smaller within these boundary layers than in the outside flow. On the rotor blades the opposite is the case. In this way a radial flow arises which may affect the efficiency of the engine appreciably. Again a Grashof number may be built as a characteristic value determining this flow. Here the radial flow is not generated by temperature differences but by the centrifugal forces immediately. Therefore, the thermal buoyancy force (per unit volume) $\gamma\beta\Delta T$ which is responsible for the thermal free convection flow is to be replaced by the centrifugal force per unit volume $\rho U^2/r$. In this way the Grashof number becomes

$$Gr = \frac{U^2 \ell^3}{r \nu^2} \qquad (36)$$

Since in applying the dimensional analysis which leads to the dimensionless characteristic numbers (Gr) it is always necessary to consider geometrically similar arrangements, one length (ℓ) can be replaced by any other (r) in the characteristic values. So the Grashof number may be written in the form

$$Gr = \frac{U^2 \ell^2}{\nu^2} \qquad (37)$$

In this form it becomes obvious that basically the Grashof number is nothing else than the square of a Reynolds number.

11. Summary

Heat transfer in thermal free convection of air was investigated with the help of a Zehnder-Mach interferometer on bodies with different shapes. All forms had in common that the convection flow set up was two-dimensional. They were: a vertical plate, two parallel vertical plates — both or only one heated, horizontal cylinders with circular and square cross-section, arrangements of two and three horizontal cylinders, and an air space enclosed between two horizontal concentric cylinders. The single horizontal cylinder and the vertical plate in free convection were thoroughly investigated experimentally by other authors and mathematical solutions are available. They are therefore convenient for checking the accuracy of the interferometric method in heat transfer investigation. It is shown that the consistency of the results gained with this method among themselves and the agreement to the previous investigations are very good. No extensive investigations are known for the other shapes and arrangements and new knowledge was derived from the interference photos. This knowledge can be applied in the field of aeronautics to cooling and isolating problems connected with the handling of special fuels. Thermal free convection data are useful also for the study of cooling problems in gas turbines and radial flow phenomena in turbo machinery. The relationship between these is discussed in detail in a special section.

BIBLIOGRAPHY

Reference No.

1. E. Eckert, R. Drake and E. Soehngen
Manufacture of a Zehnder-Mach Interferometer
AAF Technical Report 5721 (1948).

2. R. B. Kennard: An optical method for measuring temperature distribution and convection heat transfer.
National Bureau Standards Journal of Research, Vol. 8 (1932) pp. 787/805.

3. R. B. Kennard: Temperature distribution and heat flux in air by interferometry in "Temperature, its Measurement and Control in Science and Industry" pp. 685/706, Reinhold, New York 1941.

4. L. A. Ramdas and M. K. Tranjpe: An Interferometric method of measuring temperature and temperature gradients very close to a hot surface.
Current Science, Vol. 4 (1936) pp. 442/44.

5. G. Hansen: "Ueber ein Interferometer nach Zehnder-Mach (An interferometer according to Zehnder-Mach) Zeitschr. Techn. Physik, vol. 12 (1931) pp 436/40.

6. H. Schardin: Theorie und Anwendung des Mach-Zehnderschen Interferenz-Refraktometers.
Ztschr. f. Instrumentenkunde, vol. 53 (1933) pp 396/403, 424/436.

7. International Critical Tables, Vol. VII
Mac Graw-Hill, New York 1930.

8. W. F. Durand: Aerodynamic Theory, Vol. I p. 197, J. Springer, Berlin 1934.

10. E. Schmidt and W. Beckmann: Das Temperatur-und Geschwindigkeitsfeld vor einer Waerme abgebenden senkrechten Platte bei natuerlicher Konvektion
Techn. Mechanik und Thermodynamik, vol. 1 (1930) pp 341/64.

11. K. Jodlbauer: Das Temperatur-und Geschwindigkeitsfeld um ein geheiztes Rohr bei freier Konvektion. "Forschung Ing. Wesen" vol. 4 (1933) pp 157/72.

12. R. Hermann: Wärmeuebergang bei freier Stroemung am wagrechten Zylinder in zweiatomigen Gasen.VDI - Forschungsheft 379 (1936).

13. W. Beckmann: Die Wärmeuebertragung in zylindrischen Gasschichten bei natuerlicher Konvektion. Forschg. Ingenieurwes. vol. 2 (1931) pp 165/78. 213/19.

14. E. Schmidt: Moeglichkeiten der Gasturbine als Flugzeugantrieb.
Schriften d. Akad. d. Luftfahrtforschung 1055/42.

15. E. Eckert: Proposal for model tests with blade cascades for the purpose of exploring flow and heat transfer on cooled turbine blades.
Progress Report IRZ-56, Intelligence, Air Materiel Command, Wright Field (1946)